3D curvature-based tip load estimation for continuum robots

Matyas A. Diezinger[1], Brahim Tamadazte[2], and Guillaume J. Laurent[1]

***Abstract*—This letter presents a method intended for the estimation of external force and moment applied at the tip of thin rods using vision-based shape measurements, with a view to be applied on continuum robots. A versatile vision process is developed that does not require any additional markers nor sensors to provide an accurate tri-dimensional reconstruction of the deformable rod shape. Then, the tip loads (i.e., forces and moments) are directly deduced from the curvature along this curve formed by deformed rod thanks to the resolution of a linear system without requiring any iterative optimization. The curvature is determined with a robust method that allows filtering out measurement noise and artifacts. Simulations show that this approach gives fast and precise results in both 2D (planar forces estimation without torsion) and 3D (spatial forces estimation). Experimental results on cantilever rods demonstrate an accuracy of 2.2% and 2.7% of the applied forces and moments, respectively.**

***Index Terms*—Deformable rods, continuum robots, small-scale robots, force and moment estimation, stereo-vision, 3D reconstruction.**

I. INTRODUCTION

CONTINUUM Robots (CRs) have the potential to be used in a wide range applications, from medical to industrial. Unlike standard robots, CRs are made of slender flexible elements in place of rigid links. Numerous CRs have been proposed in the past few years [1], [2]. There is a common consensus that CRs offer several advantages over conventional architectures, e.g., their slender shapes as well as their potential to be miniaturized [3] allow them to reach thinly accessible area inside human bodies [2] or inside machines (turbine engines for instance). Indeed, the removal of mechanical joints allows downing size all the structure and to provide six Degrees of Freedom (DoF) with robots having diameters of a few millimeters [4]. Additionally, the compliant nature of CRs confers safer interactions with humans for collaborative tasks in industry or for medical applications [5].

Conversely, the flexibility of CRs reduces the forces and moments that can be obtained at their end-effector. The payload of these robots is also much lower than their rigid counterparts. The most serious limitation is to guarantee the robot trajectory under different loads, i.e., under various applied external forces and moments. Traditional models of CRs are based on Cosserat rod theory [6], [7] and allows calculating the actuators positions/angles to reach a desired pose in the Cartesian space. However, in the case where the external loads are not known, the models cannot predict the end-effector position. Indeed, the pose of CRs is highly dependent on unpredictable external interactions. This leads to a load-dependent trajectory that limits the capabilities of the robot. However, the compliant nature of CRs can also be used as an advantage during the design of a control strategy. As their deformations are the direct reflection of external forces, their shapes can be used to estimate these interactions. This approach has been investigated using different deformation sensors as Bragg fibers [8], [9], [10] or cable tension sensors [11].

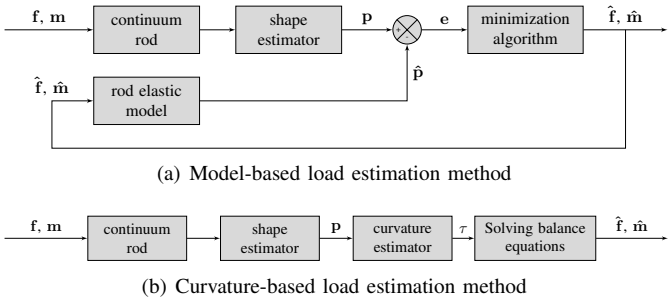

(a) Model-based load estimation method

(b) Curvature-based load estimation method

Fig. 1: Load estimation from shape ($\mathbf{f}$, $\mathbf{m}$, $\mathbf{p}$, $\mathbf{e}$ are force, moment, position and position error vectors, respectively).

Although the use of proprioceptive sensors can be the solution in certain configurations or applications, their integration on a CR is not straightforward, especially at small scale. Robots deformations are then more easily estimated by exteroceptive sensors. Among these sensors, one can imagine the use of magnetic sensors [12], cameras [13], X-ray imaging [14], optical-coherence tomography [15] as well as ultrasound imaging [16]. It is recognized that approaches that utilize a vision system may be easier to implement, more versatile, less constraining and more suitable for certain applications.

Generally, vision-based force estimation methods require first to estimate the deformation of the CR. Then, from the measured shape, the two usual ways of estimating external loads are model-based and curvature-based methods as depicted in Fig. 1. Model-based methods consist of the use of the rod deformation models coupled with iterative optimization procedures. The principle is to create a system-

This work was supported by by the French ANR program μSpider (ANR-19-CE33-0002-02), Région de Bourgogne-Franche-Comté, Equipe ROBOTEX network (ANR-10-EQPX-44-01), and EUR EIPHI program (ANR-17-EURE-0002).

[1] M. Diezinger and G. Laurent are with FEMTO-ST Institute, Univ. Bourgogne Franche-Comté, CNRS, Besançon, France. matyas.diezinger@femto-st.fr, guillaume.laurent@ens2m.fr

[2] B. Tamadazte is with Sorbonne Université, CNRS UMR 7222, INSERM U1150, ISIR, F-75005, Paris, France. brahim.tamadazte@cnrs.fr

Digital Object Identifier (DOI): see top of this page.

TABLE I: Accuracy comparison of tip force estimation on cantilever rods and catheters (single planar bending).

Related work	Sensor	Method	Object dimensions (mm)	Mean relative error
Back et al. [17]	Vision	Curvature-based	L130 × Ø3	10% of applied magnitude
Hasanzadeh et al. [18]	CMM machine	Model-based	L70 × xØ2.33	11.4% of average magnitude
Khan et al. [8]	Bragg fibers	Curvature-based	L210 × Ø0.25	6.9% of applied magnitude
Aloi et al. [19]	Vision	Model-based	L200 × Ø1.4	6.7% of average magnitude
Hooshiar et al. [14]	Vision	Curvature-based	L40 × Ø6	7.5% of maximum magnitude
Al-Ahmad et al. [10]	Bragg fibers	Model-based	L170 × Ø2.16	5.5% of applied magnitude
Xiao et al. [9]	Bragg fibers	Curvature-based	L290 × Ø1.4	5.25% to 12.87% of applied magnitude
Proposed method	**Stereo-vision**	**Curvature-based**	**L150 × Ø1**	**2.2% of applied magnitude**

like model that predicts deformations from desired external forces, and to make them converge by reducing errors between the predicted and the measured shapes. The model-based methods are usually based on the Cosserat theory [19], [10], or on simpler piece-wise constant curvature models [18] among others. However, these approaches are often slow because of model integration and challenging iterative optimization process. They also have some difficulties to converge with 3D and large deformations because the inverse problem is often ill-conditioned [19].

On the contrary, curvature-based methods are not iterative and do not require the integration of any differential equations. They can provide more robust estimations with fast computation time. The concept is to find an estimator that links the measured shape straight to internal forces and moments (Fig. 1b). Then, the external loads are estimated by solving the balance of forces and moments in several points of the CR. Obviously, this method is perfectly adapted to CRs that embed Bragg fibers as illustrated in the recent work [9]. However, some studies have also been performed with vision-based shape estimation. For instance, in [17], the curvature-based estimation is applied with a continuum robot constrained in planar motion yielding an interesting result because the obtained estimation error is approximately 10% of the applied force. The same order of estimation error is reported in [14] using real-time x-ray imaging and Bézier curve smoothing.

Both methods require a precise and robust shape measurement method. Probably one of the most challenging tasks in CRs force estimation methods is the handling of three dimensional external forces. Most of the above-mentioned works deal with planar deformations and loads, generally yielding an external force estimation with error between 5% and 10% of the applied magnitude as reported in Table I. Additional methods dealing with 2.5D configurations (i.e., slightly extra-planar loads, however quasi-planar deformations) [8], [9] reported similar performances in terms of accuracy and robustness. In fact, the tri-dimensional deformations lead to increased complexity in the force estimation for various reasons including: the challenging accurate reconstruction of the 3D deformations, the necessary estimation of the torsion, the ill-conditioning issues, etc. One of the most advanced works dealing with the estimation of 3D external forces is probably the one reported in [10] yielding an accuracy of approximately 5.5% using several Bragg fibers embedded along the deformable rod.

In this letter, we set up an accurate and versatile 3D reconstruction method suitable for all shapes and sizes of thin rods without any additional visual markers nor embedded sensors. Then, we develop a curvature-based approach to estimate the 3D tip forces on a longitudinal deformable structure based on direct measurement of its shape. The tip external loads are estimated assuming a thin continuum rod subject to no external distributed forces and that it is linearly elastic, homogeneous, and isotropic. Also, the proposed force estimation method is real-time and does not require any simulations nor optimization procedures usually used for such a problem whose performances depend directly on the proper conditioning of the optimizer. The developed force estimation method robustly filters out measurement noise and artifacts. One of the main advantages of the proposed method is the ability to work in 2D (planar forces estimation without torsion) and 3D (spatial forces estimation) configurations. Finally, the proposed method and material were successfully evaluated both numerically and experimentally.

The remainder of this paper is organized as follows. In Section II, we introduce the stereo-vision-based framework for 3D reconstruction of unknown shape rods. Section III presents the developed method for forces estimation on longitudinal deformable structure. The numerical validation of the proposed methods and materials is discussed in Section IV, when the experimental validations are presented in Section V. Finally, Section VI discusses the pros and cons of the proposed methods and materials.

II. 3D SHAPE RECONSTRUCTION OF RODS BY STEREOVISION

The first step of the proposed forces estimation approach consists of the shape reconstruction of the CR. Thus, this section deals with the tri-dimensional reconstruction of longitudinal deformable structures (e.g., rods) using a stereovision system and the epipolar geometry principles.

A. Epipolar Geometry

The stereovision system consists of a pair of standard cameras placed remotely in a manner to visualize the deformable structure with a given angle of view for each camera (approximately, 30°) (Fig. 2). Therefore, the cameras provide a pair of images of the rod to be reconstructed as a set of n measured 3D positions $\mathbf{p}(s_i)$ for $i = 1, ..., n$ at arc length position s_i.

It can be noticed that most of continuum robots are made of uniform and monochrome materials (e.g., Nitinol, certain polymers, etc.) which raises the problem of the lack of visible and recognizable visual features that can be easily and accurately detected, matched and tracked over time. By the way,

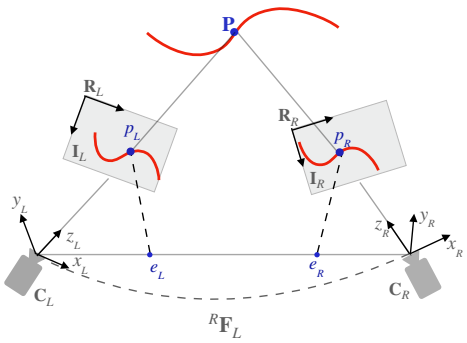

Fig. 2: Illustration of the built stereovision system used to reconstruct the 3D shape of a rod.

although it is possible to consider adding artificial markers, it is often difficult to integrate them on the continuum robot due to the size and the incompatibility with numerous applications. Hence, we investigated a method for 3D reconstruction that does not require visual markers or *a priori* knowledge of the viewed rod. This method is based on the use of the well-established epipolar geometry principle [20] as well as image processing methods easy to set up and sufficiently robust and accurate.

1) Setup configuration and involved notations: Starting with the introduction of the built stereovision system as well as the notations involved in the 3D reconstruction algorithm. Let us consider two cameras $\boldsymbol{c}_R$ and $\boldsymbol{c}_L$ with optical centers $\boldsymbol{o}_R$ and $\boldsymbol{o}_L$ viewing a 3D point $\mathbf{p} = (x, y, z)^\top$) which is projected as 2D image points $\boldsymbol{p}_L = (\boldsymbol{x}_L, \boldsymbol{y}_L)^\top$ and $\boldsymbol{p}_R = (\boldsymbol{x}_R, \boldsymbol{y}_R)^\top$, in image plans $\mathbf{I}_R$ and $\mathbf{I}_L$, respectively. The line $(\boldsymbol{o}_R\ \boldsymbol{o}_L)$ between both the camera optical centers defines the stereovision system baseline. The intersections of the baseline with the image planes give the so-called epipolar points (or epipoles) $\boldsymbol{e}_L$ and $\boldsymbol{e}_R$, when the lines $(\boldsymbol{e}_R\ \boldsymbol{p}_R)$ and $(\boldsymbol{e}_L\ \boldsymbol{p}_L)$ are known as epipolar lines. Therefore, each 2D point $\boldsymbol{p}_L$ in the left image is mathematically related to the epipolar line $(\boldsymbol{e}_R\ \boldsymbol{p}_R)$ in the right image and *vice-versa*.

The intrinsic parameters of both the $\boldsymbol{c}_R$ and $\boldsymbol{c}_L$ are defined with the matrices $\mathbf{K}_R$ and $\mathbf{K}_L$, respectively, when the extrinsic parameters that represents the pose of cameras in a common reference frame is defined as the 3D transformation ${}^R\mathbf{T}_L$ between the poses of camera $\boldsymbol{c}_R$ and camera $\boldsymbol{c}_L$. This transformation includes a 3×3 rotation matrix ${}^R\mathbf{R}_L$ and a 3×1 translation vector ${}^R\mathbf{t}_L$.

2) Epipolar projection model: The relations between a world point $\mathbf{p}$ and its two projections on the left and right images $\boldsymbol{p}_i\ i \in [R, L]$ can be expressed as follows for both the right and left cameras, respectively:

$$[\tilde{\boldsymbol{p}_L}]_\times \mathbf{K}_L\ [\mathbf{I}_{3\times3} \mid \mathbf{0}_{3\times1}]\ \tilde{\mathbf{p}} = \mathbf{0} \quad (1)$$

$$[\tilde{\boldsymbol{p}_R}]_\times \mathbf{K}_R\ [\mathbf{I}_{3\times3} \mid \mathbf{0}_{3\times1}]\ {}^R\mathbf{T}_L\ \tilde{\mathbf{p}} = \mathbf{0} \quad (2)$$

where $\mathbf{I}_{3\times3}$ is a 3×3 identity matrix, $\mathbf{0}_{3\times1}$ a 3×1 null-matrix, $\tilde{\boldsymbol{p}}_i = (\boldsymbol{p}_i, 1)^\top$ and $\tilde{\mathbf{p}} = (\mathbf{p}, 1)^\top$ are the homogeneous coordinates of $\boldsymbol{p}_i$ and $\mathbf{p}$, respectively, and $[\ \ ]_\times$ is a 3×3 skew-symmetric matrix representing a vector cross-product.

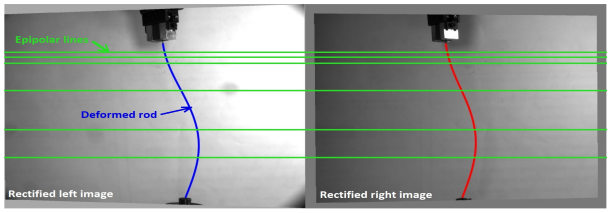

Fig. 3: Correlation process on rectified images of a rod.

Furthermore, note that both the camera intrinsic and extrinsic parameters are obtained one time and offline using a well-known camera calibration toolbox such as the one reported in [21].

3) Rectification: In order to simplify the problem of matching left and right image points, it is useful to perform a rectification procedure of the images in order to make the epipolar lines, in both the right and left images, perfectly horizontal with respect to the images frames. This means that both $\boldsymbol{e}_R$ and $\boldsymbol{e}_L$ are located at infinity. Therefore, each image point in the right image has its match in the left image along the same horizontal epipolar line, which makes the matching process much easier (Fig. 3).

4) Correlation: Once the rectification is done, it becomes trivial to determine and match the rod points between the right and left images. Both functions are performed using a conventional zero-mean normalized cross correlation (ZNCC) method [22]. With x, y defining an image reference frame in pixels, the correlation error is computed at fixed line x as following:

$$\epsilon(x_0, x) = \min_{\alpha,\beta} \frac{\sum_y |\alpha \mathbf{I}_{\mathrm{Lc}}(x, y-\beta) \mathbf{I}_{\mathrm{Lc}}(x_0, y)|^2}{\sum_y |\mathbf{I}_{\mathrm{Lc}}(x_0, y)|^2} \quad (3)$$

where x_0 is the index of the first line crossing the rod, x is the current line index, α is the correlation coefficient and β is the transverse offset from which the disparity is computed.

Indeed, for each point $\boldsymbol{p}_{i\mathrm{L}}\ (i = 1, \cdots, n)$ in the left rectified image $\mathbf{I}_{\mathrm{Lc}}$, we search the corresponding point $\boldsymbol{p}_{i\mathrm{R}}$ in the right rectified image $\mathbf{I}_{\mathrm{Rc}}$ along the corresponding horizontal epipolar line to which the point belongs. Consequently, we obtain two coherent 2D curves representing the deformable rod in each image as depicted in Fig. 3.

B. Triangulation

Now, we have all the ingredients to reconstruct the rod geometry. The previous steps have led to two set of matched image-points $\boldsymbol{p}_{i\mathrm{L}}$ and $\boldsymbol{p}_{i\mathrm{R}}\ (i = 1, \cdots, n)$, and an off-line estimation of both the intrinsic and the extrinsic parameters. Using these elements, the complete shape of the rod can be reconstructed using equations (1) rewritten as $\mathbf{A}_1\ \tilde{\mathbf{p}} = 0$ and equation (2) rewritten as $\mathbf{A}_2\ \tilde{\mathbf{p}} = 0$ combined as a unique equations system $\mathbf{A}\ \tilde{\mathbf{p}} = 0$ with $\mathbf{A} = \begin{bmatrix} \mathbf{A}_1 \\ \mathbf{A}_2 \end{bmatrix}$.

As reported in [20], the resolution of this system can be tackled by computing the eigenvectors of the built system of equations. The solution is found using a singular value

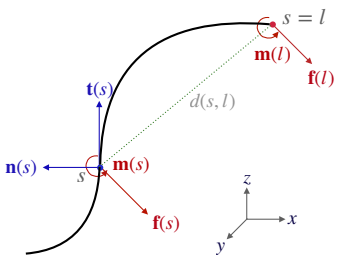

Fig. 4: Illustration of the balance between external force and moment.

decomposition (SVD) of matrix $\mathbf{A}$, giving a good estimation of the 3D point $\mathbf{p}$.

Each pair of matched points leads to a new spatial position with increasing y coordinate. At the end of the process, n points $\mathbf{p}(s_i)$ at arc length position s_i are estimated, describing the complete 3D shape of the rod.

III. LOAD ESTIMATION FROM RODS SHAPES

With a view to the initial objective of estimating external loads at the tip of a rod by measuring the induced deformation, the following section deals with the setting up of the curvature-based method.

A. Problem Statement

We consider continuum rod subject to large deformations with proper mechanical properties. These properties as well as the initial straight configuration are supposed to be known. We assume that no distributed forces or moments are applied along the rod except its own weight. Punctual force and moment localized at rod tip are responsible for large shape deformations. The section dimension is small compared to length so that the rod is considered uni-dimensional (beam length to thickness ratio of the order 20 or more). The shearing forces are then negligible compared to bending and twisting moments. Moreover, the material of the rod is assumed linearly elastic, homogeneous, and isotropic.

Let us consider a rod whose 3D shape is defined as a set of n measured 3D positions $\mathbf{p}(s_i)$ for $i = 1..n$ at arc length position s_i. Its proximal and distal ends are located at arc length 0 and l (Fig. 4), respectively. The rod is at static equilibrium, therefore the pose of each point of the rod is the image of the local moment due to external load forces.

B. Tip Force Estimation

The external force and moment are not measurable at a single point on a CR. But the 3D shape of the robot gives multiple images of the local moment due to external loads. The static equilibrium of the moments is relied upon to deduce these forces and moments. The static state of the rod implies balanced forces and moments. Then, given a point of the rod located at the arc length position s, the moments applied to the portion $[s, l]$ are balanced at s as follows:

$$\mathbf{m}(l) + \mathbf{d}(s,l) \times \mathbf{f}(l) + \mathbf{w}(s) - \mathbf{m}(s) = 0 \tag{4}$$

where $\mathbf{w}(s) = \int_s^l \mathbf{d}(s,u) \times \mathbf{g}\, \rho a \, \mathrm{d}u$ is the moment contribution induced by the mass of the rod portion $[s, l]$ and:

- a is the section of the rod;
- $\mathbf{d}(s, l)$ is the formed vector from $\mathbf{p}(s)$ to $\mathbf{p}(l)$;
- $\mathbf{f}(s)$ is the external force located at s;
- $\mathbf{g}$ is the local acceleration of free fall;
- $\mathbf{m}(s)$ is the external moment located at s;
- ρ is the linear mass of the rod;

The unknown tip load is expressed in (4) by the rod-end moment $\mathbf{m}(l) = (m_x, m_y, m_z)^\top$ and force $\mathbf{f}(l) = (f_x, f_y, f_z)^\top$ (Fig. 4). Note that each 3D reconstructed point $\mathbf{p} = (x, y, z)^\top$ of the rod yields three equations (one per axis), then at least two points are necessary to estimate the six unknowns of the tip load. However, for better precision and robustness to measurement errors, it is highly recommended to consider a larger number of reconstructed 3D points.

Thereby, (4) can be rewritten as a redundant linear system of equations in the form of $\mathbf{Ax} = \mathbf{y}$:

$$\overbrace{\begin{bmatrix} [\mathbf{d}(s_0, s_k)]_\times & \mathbf{I}_{3\times3} \\ \vdots & \vdots \\ [\mathbf{d}(s_n, s_k))]_\times & \mathbf{I}_{3\times3} \end{bmatrix}}^{\mathbf{A}} \cdot \overbrace{\begin{bmatrix} \mathbf{f}(l) \\ \mathbf{m}(l) \end{bmatrix}}^{\mathbf{x}} + \overbrace{\begin{bmatrix} \mathbf{w}(s_0) \\ \vdots \\ \mathbf{w}(s_n) \end{bmatrix} - \begin{bmatrix} \mathbf{m}(s_0) \\ \vdots \\ \mathbf{m}(s_n) \end{bmatrix}}^{-\mathbf{y}} = 0 \tag{5}$$

To solve the system (5), a QR decomposition is used in order to transform the matrix $\mathbf{A}$, as product of an orthogonal matrix $\mathbf{Q}$ and an upper triangular matrix $\mathbf{R}$ (i.e., $\mathbf{A} = \mathbf{QR}$). Therefore, the problem can be tackled by a backwards substitution technique.

Building the system (5) requires a set of position of 3D points reconstructed using the proposed method, and a set of local moments that can be estimated from these positions as discussed below.

C. Local Moment Estimation

On a 3D curve, the local section orientation follows the deformations. Let that orientation be given by the Frenet-Serret frame formed at each position $\mathbf{p}(s)$ by the tangent unit vector $\mathbf{t}(s)$, the normal unit vector $\mathbf{n}(s)$, and the binormal unit vector $\mathbf{b}(s)$ obtained as the cross product of $\mathbf{t}(s)$ and $\mathbf{n}(s)$. The triplet of vectors are obtained as follows:

$$\mathbf{t}(s) = \frac{\mathbf{p}'(s)}{\|\mathbf{p}'(s)\|} \tag{6}$$

$$\mathbf{n}(s) = \frac{\mathbf{t}'(s)}{\|\mathbf{t}'(s)\|} \tag{7}$$

$$\mathbf{b}(s) = \mathbf{t}(s) \times \mathbf{n}(s) \tag{8}$$

The rod deformations are given by the curvature κ and the torsion τ that represent the flexion and the twist, respectively. The curvature is the deviation of the tangent from a straight direction, locally following a circular arc. In other words, the inverse radius of this arc is the curvature. The plane containing this arc is named the osculating plane and contains by definition the tangent vector $\mathbf{t}(s)$ and the normal vector $\mathbf{n}(s)$. The torsion τ is the angular spatial velocity of the osculating plane, i.e. the angular velocity of its normal $\mathbf{b}(s)$.

The curvature and the torsion are defined, respectively, as follows:

$$\kappa(s) = \|\mathbf{t}'(s)\| \tag{9}$$

$$\tau(s) = \|\mathbf{b}'(s)\| \tag{10}$$

The deformations are directly related to the local moments $\mathbf{m}(s)$ through stress-strain constitutive laws which are expressed as follows:

$$\mathbf{m}(s) = \mathrm{EI}\kappa(s)\mathbf{b}(s) + \mathrm{GJ}\tau(s)\mathbf{t}(s) \tag{11}$$

where E is the Young's modulus, I is the quadratic moment of area along radial direction, G is the shear modulus, and J is the torsion constant (quadratic moment of area along axial direction).

D. Discrete Curvature and Torsion Estimation

The computation of the local moment uses the estimation of the tangent and binormal vectors as well as the curvature and torsion. All these elements can be defined from the positions $\mathbf{p}(s)$ and its three first derivatives [23]. However, although the 3D reconstruction method is accurate, the deformation estimation is sensitive to measurement noise, especially emphasized by the use of derivatives. Indeed, the evaluation of discrete curvature and torsion from position is challenging and has been addressed in several ways such as B-spline smoothing [24] or weighted least-squares curve fitting [25].

To avoid the use of 3-order spatial derivatives, the curvature and the torsion can alternatively be estimated from the osculating plane and its rotation rates around the tangent vector as proposed by [26]. This method is more robust to measurement noise and its implementation is available for MATLAB[1].

In order to tackle the induced measurement noise, the Frenet frame estimation is performed on a sliding window centered at each curvilinear abscissa s_i. The rod section considered in the sliding window is centered on the origin to form the 3D points set $\mathbf{P}$ defined as follows:

$$\mathbf{P}(s_i) = \left[\mathbf{p}(s_{i-k}) - \overline{\mathbf{p}(s_i)}, \quad \cdots, \quad \mathbf{p}(s_{i+k}) - \overline{\mathbf{p}(s_i)}\right] \tag{12}$$

where $\overline{\mathbf{p}(s_i)}$ is the centroid of positions neighbouring $\mathbf{p}(s_i)$.

The eigenvectors of the matrix $\mathbf{P}(s_i)$ provide a frame attached to the estimated set of points. These are estimated with a singular value decomposition shown in (13). $\mathbf{U}(s_i)$ and $\mathbf{V}(s_i)$ are the projective matrices and $\mathbf{D}(s_i)$ is the diagonal matrix containing the eigenvalues. These eigenvectors are the columns of $\mathbf{U}(s_i)$ and the tangent $\mathbf{t}(s_i)$ is given by the vector with greatest eigenvalue, as in a usual line correlation. The second greatest value gives the estimation of the normal $\mathbf{n}(s_i)$, while the third that of the estimation of the binormal $\mathbf{b}(s_i)$.

$$\mathbf{P}(s_i) = \mathbf{U}(s_i)\mathbf{D}(s_i)\mathbf{V}(s_i)^\top \tag{13}$$

The tangent and normal vectors $\mathbf{t}(s_i)$ and $\mathbf{n}(s_i)$ define the osculating plane at s_i. The curvature $\kappa(s_i)$ is then determined as the inverse of the radius of the best fitted circle in the osculating plane using Taubin's method [27].

[1]https://de.mathworks.com/matlabcentral/fileexchange/47885-frenet_robust-zip

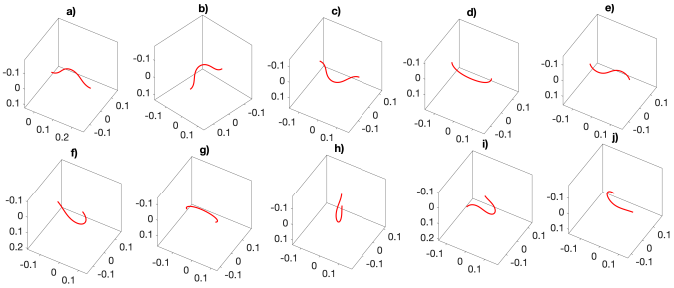

Fig. 5: Examples of simulated rods with given density (2000kg.m^{-3}), young modulus (81GPa), shear modulus (32GPa), radius (0.5mm), length (260mm) and number of points (50).

Concerning the torsion $\tau(s_i)$, it corresponds to the rotation rate of the osculating plane.

As the rotation of the osculating plane is continuous, the angle between consecutive normal vectors remains small which can be either positive or negative. Therefore, the torsion is computed using the normal and the binormal at the previous position s_{i-1} as follows:

$$\tau(s_i) = \frac{\arcsin\left(\mathbf{b}(s_{i-1}) \cdot \mathbf{n}(s_i)\right)}{s_i - s_{i-1}} \tag{14}$$

The continuity of the normal and the binormal directions is ensured by avoiding flips that can occur on parts of the rod with zero curvature. Therefore, the normal vector does not always points toward the center of the osculating circle, which results in a negative curvature.

IV. NUMERICAL VALIDATION

The validation of the rod tip forces and moments estimation method goes through the evaluation of various 3D rods. To do this, it is necessary to numerically generate a data-set of different shaped rods. Also, the simulated rods allow evaluating all the state variables, particularly the internal moments.

The generation of several theoretical rod shapes is carried out with the robust finite element modeler available within the open-source simulation framework SOFA dedicated to modelling of deformable objects [28]. Several 3D rod shapes are generated (Fig. 5) to cover different possible rod deflection shapes.

Our force estimation method was then evaluated on the different 3D obtained shapes depicted in Fig. 5. The estimated forces and moments are compared to the theoretical ones as can be seen in Fig. 6. As can be highlighted in this figure, the estimated forces almost overlap the theoretical ones in most of the configurations. From a numerical point of view, the force estimation gives an average error of 0.062N (respectively, a maximum error of 0.26N) within a range of 2.6N, while the moment estimation gives an average error of 0.0044N.m (respectively, a maximum error of 0.0068N.m) within a range of 0.13N.m.

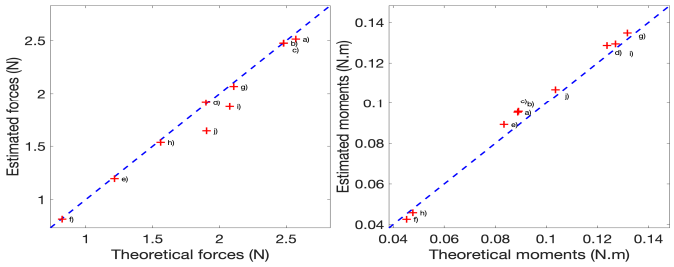

Fig. 6: Comparison of estimated tip force and moment with theoretical ground values for the ten simulated rods of Fig. 5.

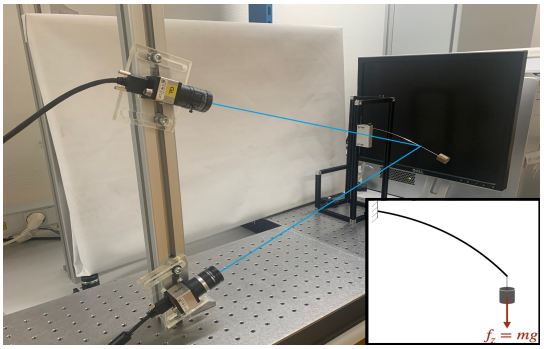

Fig. 7: Vision setup with cantilever rod.

V. EXPERIMENTAL VALIDATION

A. Shape Reconstruction Validation

1) Vision setup: The used cameras to build the stereovision system consist of two IDS cameras (version: UI-3481LE-M-GL) providing 2560×1920 pixels at the rate of 15 frames/second. The cameras were mounted in such a way to obtain an angle of about 30 degrees from one camera to another (offering a good quality of triangulation for 3D reconstruction), a baseline of 30cm and a working distance of 50cm from the observed scene (Fig. 7). In order to increase the contrast between the rod and the background and thus facilitate the image processing tasks (e.g., the correlation-based matching method), a homogeneous light source illuminating in the axis of the cameras was used. Both the 3D reconstruction algorithms and the force estimation approach were implemented in Win PC equipped with an Intel Core i5 processor.

2) Shape estimation: The 3D reconstruction process has been tested on different single rods with various 3D shapes, diameters of the rod (0.25mm to 2mm) and materials (steel, glass and plastic). It has been demonstrated that the designed stereo-vision setup as well as the reconstruction algorithms are able to provide accurate three-dimensional information of the observed rod. The only condition to fulfill is to ensure that there is enough contrast between the observed rod and the background to guarantee a good matching between the information detected in both the left and the right images.

B. Model Validation

In order to verify the model, an experimental validation process is conducted with a carbon fiber beam deformed to four different shapes with known tip orientation and position. The characteristic features of the rod as the length (L = 260mm) and the radius (R = 0.5mm) are measured using caliper with an accuracy of 10μm, when the density (d = 3032kg.m^{-3}) is obtained thanks a precision scale with an accuracy of 0.01mg. Concerning, the Young modulus (E = 80GPa) and shear modulus (G = 32GPa) are provided by the manufacturer but also confirmed by three-point bend tests realized in our facility.

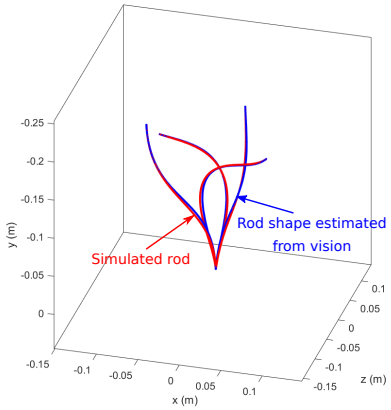

Fig. 8: Rods simulated from real rod end poses.

The shape is reconstructed by vision and compared to a theoretical rod shape generated with SOFA from the same parameters (Fig. 8). SOFA is a finite element-based software dedicated to dynamic continuum mechanics simulation widely used by the soft robotic community. Specifically, the SOFA model allows validating the coherence and the reliability of both the vision process and the measured rod parameters used for the generated model. However, as can be seen in Fig. 8, there is a very small shift between the reconstructed rods and the simulated ones. Two potential origins of error are envisaged: 1) the existence of an initial curvature/stress (not considered in the model) when the rod is initially considered perfectly straight , and 2) small lateral errors in the correlation process on rectified images, due to the acquisition conditions (blur, shadow). However, these shifts between 3D real shapes and reconstructed ones remain insignificant to significantly impact the accuracy of the proposed force estimation method.

C. Moments Estimation

In order to validate experimentally the proposed force estimation method, we used a 150mm long steel cantilever rod (as depicted in Fig. 7) whose 3D shape has been reconstructed by the proposed vision method. As mentioned in Section III-D, the efficiency and accuracy of the estimation of local curvature and torsion and then the local moments depend directly on the ability to handle noise in position measurements. To highlight this, a comparison is made between Frenet bases estimated 1) from derivatives of positions after a B-Spline smoothing procedure and 2) from the fitting of the osculating plane and circle (Frenet robust).

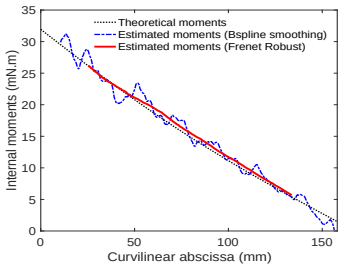

Fig. 9: Comparison of estimated internal moments magnitude in a cantilever rod.

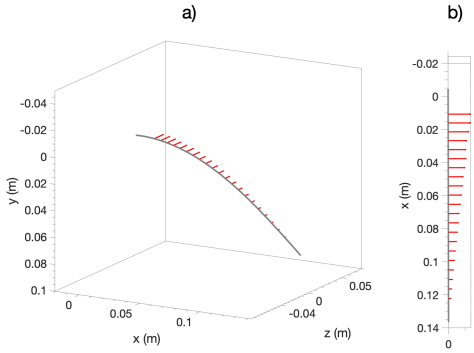

Fig. 10: a) Perspective view of the shape reconstruction of a cantilever rod with estimated internal moments, and b) a top view of the estimated internal moments.

The rod is weighted with a 0.24N load at its end so that the deformations remain planar and there is no torsion involved. The moments are then all pointing in the same direction with a decreasing magnitude. As shown in Fig. 9, the proposed method gives a more accurate estimation of the moments with an average error of 0.54mN.m and a maximum error of 0.99mN.m whereas the B-Spline smoothing method gives an average error of 1.47mN.m and a maximum error of 3.02mN.m. The local moments are represented on the reconstructed rod shape illustrated in Fig. 10.

D. Load Estimation on Cantilever Rods

The previous experiment has been conducted on five cantilever rods loaded with several masses ranging from 12.8g to 35.48g in order to validate the accuracy of the method over a large range of loads. The measured parameters are the density ($3032 kg.m^{-3}$), the young modulus (60GPa), the shear modulus (24GPa) and the radius (0.5mm). The vision process gives the length of the rod (158mm).

The forces due to the hanging weight are known and compared to the estimated forces (Fig. 11). The difference between the applied and estimated values of forces and moments are about 2.2% (with a maximum error of 4.4%) and 2.7% (with a maximum error of 5.1%) on average of the applied forces and moments, respectively. It can be highlighted that the proposed method outperforms the state-of-the-art approaches summarized in Table I. Indeed, the more advanced method [9] combines Bragg fibers as shape sensor and curvature-based method as the force estimator provides an accuracy ranging

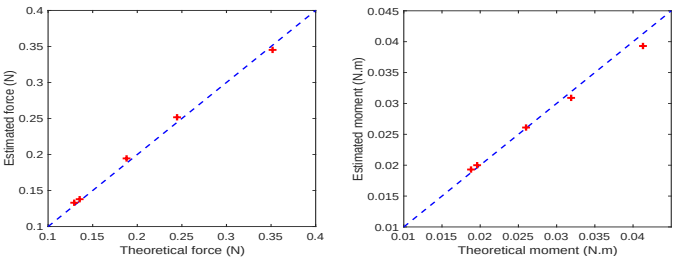

Fig. 11: Tip force and moment estimation errors on cantilever rods.

from 5.25% to 12.87% of the applied forces. On the other hand, the most relevant approaches reported in the literature using a vision method for the rod shape estimation and a curvature-based estimator [14] gives an accuracy of 7.5% of the applied forces.

E. Load Estimation from 3D Deformation

The proposed methods in this letter have been tested on a rod deformed manually on both sides of its extremities. The objective is to demonstrate the operation of the method in real conditions of use. Fig. 12 shows different rod deformations with the corresponding force and moment estimations in overlays. These experiments can be much more appreciated on the supplementary video file accompanying to this letter. These experiments illustrate the robustness of the proposed method to detect, to reconstruct and to estimate tip load in real conditions and paves the way to the force sensing/control of continuum robots. Note that the force estimation method is implemented in Matlab running at 37Hz on a Win 64 PC equipped with an Intel Core i5 processor and 16Go of RAM.

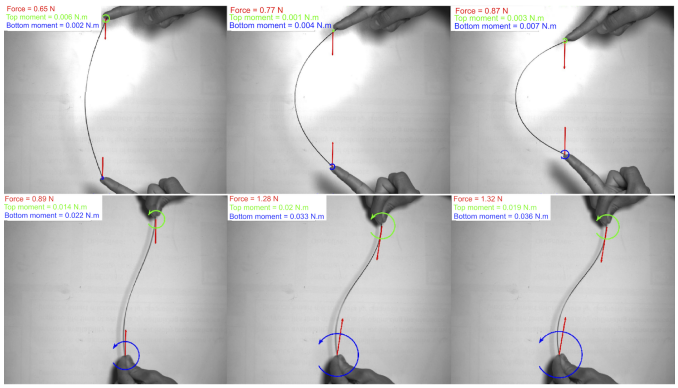

Fig. 12: Estimated forces and moments on "C-shape" rod (first row) and "S-shape" rod (second row). Additional examples can be seen in the attached multimedia materials.

VI. STRENGTHS AND SHORTCOMINGS

The purpose of this letter is to provide an accurate curvature-based method for 3D tip load (forces and moments) estimation. The main advantage of the method is to use curvature information (obtained by vision) of a deformable rod to directly and accurately estimate the tip external forces and moments

without any optimization procedure. Although the method has demonstrated good performance in terms of accuracy and robustness in particular to the rod shape measurement noise, it suffers from certain weaknesses that can be addressed in future work. Indeed, the force estimation method, relatively easy to implement, requires a good knowledge of the 3D shape of the rod resulting from the 3D reconstruction method using stereo-vision principles. However, this method is prone to the numerous uncertainties that characterize vision-based 3D reconstruction methods: time-consuming without optimized implementation (e.g., GPU), occlusion problems, blurred images, jerky motions, etc. To remedy this, it is possible to consider using integrated depth-camera such as the recent one from Intel (RealSense D405) instead of a custom stereo-vision system. Moreover, some singular configurations (e.g., straight rod) raise impossibilities in estimating the forces, namely when the applied external force is perpendicular to the section of the rod and when deformations are visible before the buckling. Indeed, the elastic deformation due to the compression force along the rod does not lead to visible deformations up to the Euler load (as can be seen in the attached video file). This compression phase before the buckling can be considered as a dead zone for the curvature estimation task and consequently for the forces estimation method. This singularity can be detected by checking if the rod deflection is above a given threshold in order to apply the proposed force estimation method. This threshold has been fixed to 0.2% of whole length for the previous experiments.

VII. CONCLUSION

In this letter, an accurate and fast method to estimate tip loads on a continuum rod based on curvature calculation has been presented. Magnitude and direction are estimated for both external forces and moments from stereo images. Simulations on various rods with large deformations showed a precision of 0.062N within a range of 2.6N in the force measurement and experimental results on cantilever rods showed an accuracy of 2.2% of applied magnitude. The method can be applied to any 3D deformations of a rod without additional visual markers nor embedded sensors. In future work, we aim to implement this method for dynamic control of a parallel continuum robot and to handle passive deformations occurring on the robot's path. This will require adding the inertial effects and thus tracking the robot's shape over time to estimate its acceleration at each point.

ACKNOWLEDGMENTS

Authors acknowledge Pierre Roux, Stani Carbillet and Michael Fontaine for their technological assistance through the AMETISTE and MIFHYSTO facilities.

REFERENCES

[1] R. J. Webster III and B. A. Jones, "Design and kinematic modeling of constant curvature continuum robots: A review," *The Int. J. of Rob. Res.*, vol. 29, no. 13, pp. 1661–1683, 2010.

[2] J. Burgner-Kahrs, D. C. Rucker, and H. Choset, "Continuum Robots for Medical Applications: A Survey," *IEEE T. on Rob.*, vol. 31, pp. 1261 – 1280, 2015.

[3] X. Dong, D. Axinte, D. Palmer, *et al.*, "Development of a slender continuum robotic system for on-wing inspection/repair of gas turbine engines," *Rob. and Comp.-Integ. Manuf.*, vol. 44, pp. 218–229, 2017.

[4] Y. Chitalia, N. J. Deaton, S. Jeong, *et al.*, "Towards fbg-based shape sensing for micro-scale and meso-scale continuum robots with large deflection," *IEEE Rob. and Auto. Let.*, pp. 1712–1719, 2020.

[5] S. Sanan and C. G. Atkeson, "Continuum robots: An approach to safer robots," in *Citeseer*, 2010.

[6] S. S. Antman, *Nonlinear Problems of Elasticity*, 2nd ed., ser. Mathematics Subject Classification, 2005, vol. 107.

[7] D. C. Rucker, B. A. Jones, and R. J. Webster, "Statics and Dynamics of Continuum Robots With General Tendon Routing and External Loading," *IEEE T. On Rob.*, vol. 27, pp. 1033 – 1044, 2011.

[8] F. Khan, R. J. Roesthuis, and S. Misra, "Force sensing in continuum manipulators using fiber bragg grating sensors," in *IEEE/RSJ Int. Conf. on Intel. Rob. and Syst.*, 2017, pp. 2531–2536.

[9] Q. Xiao and Y. Chen, "Efficient force estimation for continuum robot," *arXiv preprint arXiv:2109.12469*, 2021.

[10] O. Al-Ahmad, M. Ourak, J. Vlekken, and E. Vander Poorten, "Fbg-based estimation of external forces along flexible instrument bodies," *Frontiers in Robotics and AI*, vol. 8, 2021.

[11] M. Jolaei, A. Hooshiar, A. Sayadi, *et al.*, "Sensor-free force control of tendon-driven ablation catheters through position control and contact modeling," in *Ann. Int. Conf. of the IEEE Eng. in Med. and Biol. Soc.*, 2020, pp. 5248–5251.

[12] H. Guo, F. Ju, Y. Cao, *et al.*, "Continuum robot shape estimation using permanent magnets and magnetic sensors," *Sens. and Actua. A: Physical*, vol. 285, pp. 519–530, 2019.

[13] J. M. Croom, D. C. Rucker, J. M. Romano, and R. J. Webster, "Visual Sensing of Continuum Robot Shape Using Self-Organizing Maps," *IEEE Int. Conf. on Rob. and Auto.*, 2010.

[14] A. Hooshiar, A. Sayadi, M. Jolaei, and J. Dargahi, "Accurate estimation of tip force on tendon-driven catheters using inverse cosserat rod model," in *Int. Conf. on Biom. Innov. and Appl.)*, 2020, pp. 37–40.

[15] Y. Baran, K. Rabenorosoa, G. J. Laurent, P. Rougeot, N. Andreff, and B. Tamadazte, "Preliminary results on oct-based position control of a concentric tube robot," in *IEEE/RSJ Int. Conf. on Intel. Rob. and Sys.*, 2017, pp. 3000–3005.

[16] M. Aggravi, D. A. L. Estima, A. Krupa, *et al.*, "Haptic teleoperation of flexible needles combining 3d ultrasound guidance and needle tip force feedback," *IEEE Rob. and Auto. Let.*, pp. 4859–4866, 2021.

[17] J. Back, T. Manwell, R. Karim, *et al.*, "Catheter Contact Force Estimation from Shape Detection using a Real-Time Cosserat Rod Model," *IEEE/RSJ Int. Conf. on Intel. Rob. and Sys.*, 2015.

[18] S. Hasanzadeh and F. Janabi-Sharifi, "Model-based force estimation for intracardiac catheters," *IEEE/ASME T. on Mech.*, vol. 21, pp. 154–162, 2016.

[19] V. A. Aloi and D. C. Rucker, "Estimating Loads Along Elastic Rods," *Int. Conf. on Rob. and Auto.*, 2019.

[20] R. Hartley and A. Zisserman, *Multiple View Geometry in Computer Vision*, 2nd ed. Cambridge University Press, 2000.

[21] Z. Zhang, J. Dequidt, and C. Duriez, "Vision-Based Sensing of External Forces Acting on Soft Robots Using Finite Element Method," *IEEE Rob. And Auto. Let.*, 2018.

[22] M. Guizar-Sicairos, S. T. Thurman, and J. R. Fienup, "Efficient subpixel image registration algorithms," *Opt. Lett.*, vol. 33, no. 2, pp. 156–158, 2008.

[23] A. Pressley, "How much does a curve curve," in *Elementary Differential Geometry*. Springer Undergraduate Math. S., 2001, pp. 29–54.

[24] N. Kehtarnavaz and R. Defigueiredo, "A 3-d contour segmentation scheme based on curvature and torsion," *IEEE T. on Pat. Anal. and Mach. Intel.*, vol. 10, pp. 707–713, 1988.

[25] T. Lewiner, J. D. Gomes, H. Lopes, and M. Craizer, "Curvature and torsion estimators based on parametric curve fitting," *Computers and Graphics*, vol. 29, no. 5, pp. 641–655, 2005.

[26] A. Gong, S. Rode, G. Gompper, *et al.*, "Reconstruction of the three-dimensional beat pattern underlying swimming behaviors of sperm," *The Eu. Phys. J. E*, vol. 44, p. 87, 2021.

[27] G. Taubin, "Estimation of planar curves, surfaces, and nonplanar space curves defined by implicit equations with applications to edge and range image segmentation," *IEEE T. on Pat. Anal. & Mach. Intel.*, vol. 13, pp. 1115–1138, 1991.

[28] E. Coevoet, T. Morales-Bieze, F. Largilliere, *et al.*, "Software toolkit for modeling, simulation and control of soft robots," *Advanced Robotics*, vol. 31, pp. 1208–1224, 2017.